

Extended Barrier Lifetime of Partially Cracked Organic/ Inorganic Multilayers for Compliant Implantable Electronics

Kyungjin Kim, Matthias Van Gompel, Kangling Wu, Giuseppe Schiavone, Julien Carron, Florian Bourgeois, Stéphanie P. Lacour,* and Yves Leterrier*

Flexible and soft bioelectronics display conflicting demands on miniaturization, compliance, and reliability. Here, the authors investigate the design and performance of thin encapsulation multilayers against hermeticity and mechanical integrity. Partially cracked organic/inorganic multilayer coatings are demonstrated to display surprisingly year-long hermetic lifetime under demanding mechanical and environmental loading. The thin hermetic encapsulation is grown in a single process chamber as a continuous multilayer with dyads of atomic layer deposited (ALD) Al₂O₃-TiO₂ and chemical vapor deposited Parylene C films with strong interlayer adhesion. Upon tensile loading, tortuous diffusion pathways defined along channel cracks in the ALD oxide films and through tough Parylene films efficiently postpone the hermeticity failure of the partially cracked coating. The authors assessed the coating performance against prolonged exposure to biomimetic physiological conditions using coated magnesium films, platinum interdigitated electrodes, and optoelectronic devices prepared on stretchable substrates. Designed extension of the lifetime preventing direct failures reduces from over 5 years yet tolerates the lifetime of 3 years even with the presence of critical damage, while others will directly fail less than two months at 37 °C. This strategy should accelerate progress on thin hermetic packaging for miniaturized and compliant implantable electronics.

K. Kim, K. Wu, G. Schiavone, S. P. Lacour Bertarelli Foundation Chair in Neuroprosthetic Technology Laboratory for Soft Bioelectronic Interfaces Institute of Microengineering, Institute of Bioengineering Centre for Neuroprosthetics École Polytechnique Fédérale de Lausanne Geneva 1202, Switzerland E-mail: stephanie.lacour@epfl.ch K. Kim, J. Carron, Y. Leterrier Laboratory for Processing of Advanced Composites Institute of Materials School of Engineering École Polytechnique Fédérale de Lausanne Lausanne 1015, Switzerland E-mail: yves.leterrier@epfl.ch M. Van Gompel, F. Bourgeois Comelec SA La Chaux-de-Fonds 2300, Switzerland



The ORCID identification number(s) for the author(s) of this article can be found under https://doi.org/10.1002/smll.202103039.

© 2021 The Authors. Small published by Wiley-VCH GmbH. This is an open access article under the terms of the Creative Commons Attribution License, which permits use, distribution and reproduction in any medium, provided the original work is properly cited.

DOI: 10.1002/smll.202103039

1. Introduction

A critical challenge to overcome for the next generation of implantable electronic systems is the design, synthesis, and integration of barrier coatings that combine hermeticity, biocompatibility, and miniaturization in agreement with physiological and therapeutic timescales.[1] Advances in flexible and soft bioelectronics call for new materials and packaging strategies to accommodate thin and/or large-area formfactors, high mechanical demands, and long-term stability. Current barrier coatings for flexible electronics exploit organic films such as Teflon,^[2] polyimide (PI),^[3,4] Parylene C, [5,6] silicones, [7] and inorganic films formed from Al or Si (Al₂O₃, SiO₂, SiN_x, SiC).^[8–12] The long-term endurance of these thin coatings remains a critical aspect, and the modest in vivo reliability of flexible implantable systems limits thus far their long-term use and clinical translation that anticipates functional lifetime that exceeds 5 years in the body.[13–15]

Over the past decade, the introduction of atomic layer deposition (ALD) and high-temperature chemical vapor deposition (CVD) to form hermetic barrier materials has significantly enhanced coated device lifetime. [15] For example, Minnikanti et al. report 3 years as mean time to failure for 52 nm thin ALD Al₂O₃ on Parylene C barriers coated on silica substrate, a 4.5 time increase compared to bare Parylene C coating.[12] Jeong et al. report an equivalent lifetime of 10 years at 37 °C for 100 nm ALD HfO₂/SiO₂ multilayers coated on wirelessly powered microdevice chiplets.^[16] Thermal SiO₂ or CVD SiO_x, [8] SiN_x, and SiC films, [9,11] SiO₂/ALD HfO₂ barriers,^[17] grown at high temperature (>800 °C) then transferred onto the flexible carriers, provide extremely low water permeabilities equivalent to a projected lifetime of several decades.

While such ultrabarriers present excellent hermeticity, they offer limited elasticity due to the brittle nature of inorganic oxides. A metric describing the elastic limit of an ultrabarrier is the crack onset strain (COS), that is, the applied strain initiating crack propagation in the brittle films.^[18] COS of ultrabarriers is small: for 10 nm thick ALD Al₂O₃ films on PET substrate, it is typically 1.5-2.0 %, a value that further decreases with increasing film thickness $h_{\rm f}$ in $h_{\rm f}^{-0.5,[19-22]}$ Upon tensile loading and at COS, the thin barrier produces channel cracks perpendicular to the uniaxial loading direction (Figure 1a(1)), and rapidly loses its hermeticity.

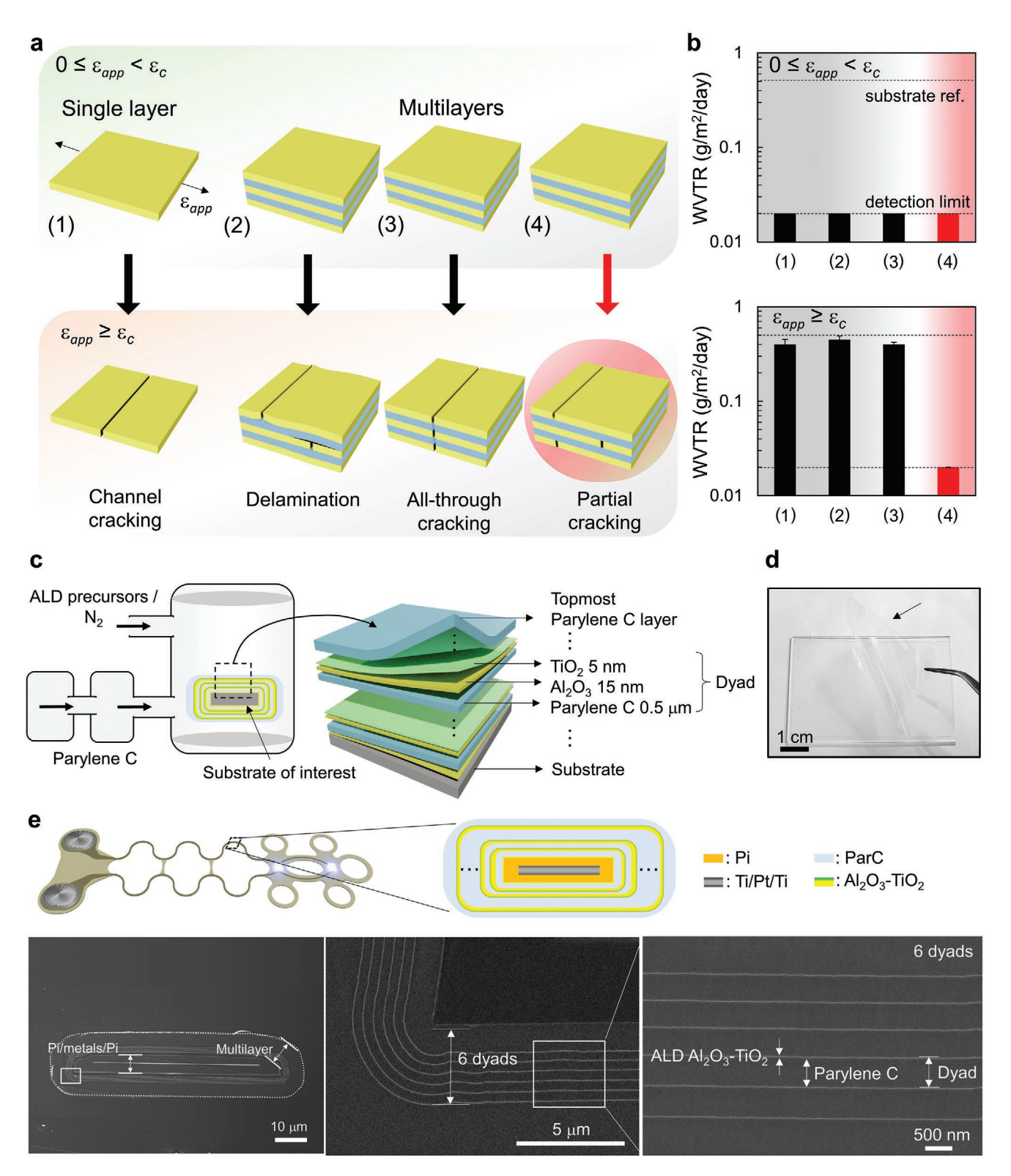


Figure 1. Organic/inorganic multilayer coatings. a) Single- and multi-layer barriers under uni-axial applied strains ε_{app} below the COS ε_c (top) and over the COS ε_c (bottom), classified for different mechanical failure modes: 1) Channel cracking. 2) Delamination triggered by poor interlayer adhesion. 3) All-through cracking at ε_c . 4) Partial cracking. b) WVTRs from (1) to (4) with (top) and without (bottom) the presence of mechanical failures. c) Schematic of the single-chamber system for continuous deposition of alternating CVD Parylene C and ALD Al₂O₃-TiO₂; 3D rendering of the resulting multilayer structure. d) Photograph of a multilayer coating peeled away from a glass slide. e) Cross-sectional SEM images of the flexible conductor conformally encapsulated with a 6-dyad Parylene C-Al₂O₃-TiO₂ coating.

Multilayer architectures consisting of alternating organic and inorganic layers (Figure 1a(2–4)) offer interesting opportunities to mitigate the conflicting challenges of designing hermetic, thin, and flexible barrier coating. The inorganic layers provide high-quality barrier properties while the organic films, usually thermoplastics, act as a mechanical buffer. Upon decoupling of the defects in inorganic layers, a tortuous pathway for diffusion of small molecules results within the layered structure and drives a major increase of the lag time for the molecules to reach the underlying functional layer or device, further slowed down with an increasing number of dyads in the barrier.^[23] Furthermore, improved COS can be designed by preserving thin inorganic layers separated by organic interlayers.^[24,25]

In this work, we report the systematic characterization of multilayered barrier coatings prepared as stacked dyads of ALD Al₂O₃/TiO₂ layer and CVD Parylene C layer continuously produced in a single vacuum chamber at low temperature. An in situ plasma treatment, applied in-between each layer growth ensures strong adhesion between the inorganic and organic films, preventing delamination (Figure 1a (2)). Furthermore, the multilayered design prevents all-through cracking (Figure 1a (3)) and supports random partial cracks (Figure 1a (4)). Barrier properties are pre-examined by measuring water vapor transmission rates (WVTRs) using a permeation analyzer (Systech Instrument 7001) with and without the presence of mechanical failures (Figure 1b). We observe systematic degradation of the WVTR levels when the films are strained beyond their COS except for the continuous multilayer coating for which the WVTR remains below our instrument detection limit, that is, 0.02 g m⁻² day⁻¹. Next, we implement a set of multimodal testing methods to predict an equivalent lifetime of the thin multilayer barrier coating in physiological conditions (saline solution, 37-67 °C). We monitor crack configurations within the multilayer barrier under in-plane stress using in situ scanning electron microscopy (SEM) to quantify eventual changes in hermeticity upon mechanical loading. We hypothesize the organic/inorganic multilayer structure remains water-tight for an extended period of time post-cracking of the inorganic films and as long as the organic interlayers and organic/inorganic interfaces stay intact.

2. 3D Hybrid Multilayer Coating

We design the multilayer structure with repeated dyads of 500 nm thick Parylene C, 15 nm thick Al_2O_3 , and 5 nm thick TiO_2 . The ultrathin TiO_2 layers are grown atop Al_2O_3 to prevent its dissolution in water.^[26] The ALD film thickness was chosen to be 15 nm as a trade-off between hermeticity and the highest COS possible.^[19–22] All barrier coatings are grown on an initial adhesion ALD Al_2O_3 layer (thinner than 5 nm) and capped with a final 6 μ m thick Parylene C film (Figure 1c).

The latter enhances the mechanical integrity of the structure and decreases its overall permeability. The deposition of the Parylene C-ALD multilayer is performed at low temperature using a novel hybrid reactor from Comelec SA (La Chaux-de-Fonds, Switzerland), which does not necessitate venting steps between the Parylene C and metal oxide ALD deposition processes. The deposition temperature is limited to 100 °C, which

is compatible with a wide range of carrier and device materials. Figure 1d shows a transparent free-standing 3-dyad barrier film peeled away from a glass substrate (76 mm \times 52 mm surface area). The regular stacking of the organic/inorganic dyads is revealed with ion polishing and electron microscopy of a cross-section of an encapsulated thin metal film (titanium/platinum/titanium, 50/320/50 nm thick) embedded in 5 μ m thick polyimide (Figure 1e). Conformability and continuity of the multi-layered coatings are striking.

3. Flexible and Stretchable Substrates with Multilayer Coatings

Next, we assess the performance of the barrier coating using encapsulated magnesium (Mg) films, interdigitated electrodes (IDEs), and micro-LEDs in bare die format interconnected with flexible metal conductors^[27] (see Experimental Section) (Figure 2a-c). Samples are immersed in saline solution at 80 °C, inspected, and tested at regular time points (in days). It is worth noting that, when we increase the frequency of data collection under electrical powering, an accelerated permeation of charged ions may further shorten the device lifetime. A substantial decrease in lifetime was observed by Xie et al. during continuous functioning: the lifetime of Parylene-Al₂O₃ bilayer coated wireless neural interfaces was reduced by a factor of >13 by applying a constant bias of 5 V (from >1860 days (still ongoing) at 37 °C to 140 equivalent days). [28] The result suggests that electrical bias stress is a significant factor that can accelerate failure of the encapsulated devices.

When Mg is exposed to water molecules, its color changes from light to dark gray as the outermost layer of magnesium oxide corrodes. We use both optical inspection of coated Mg film and monitoring of the electrical resistance of coated Mg tracks (Figure 2d–e) to estimate the barrier lifetime. We define a degradation threshold as the appearance of a dark spot of 10 to 50 μ m in diameter in the middle of the specimen (5 mm \times 3 cm). We find that the electrical resistance of Mg tracks starts to increase at the time when the corrosion sites are observed, confirming leakage of the phosphate buffer saline (PBS) solution through the multilayer coating. Furthermore, the resistance remains stable over longer period of time as the number of dyads increases (Figure 2e).

Leakage current across the IDE structures is monitored over time (Figure 2f) along with electrochemical impedance spectra (EIS) (Figure S2, Supporting Information). These results show the reliability of the multilayered coating improving with the number of dyads due to the proportional increase in the total diffusion pathways (Figure 2g). Aging factors are commonly used to extrapolate the lifetime to body temperature (37 °C) when the activation energy for the relevant degradation process is unknown. Assuming an aging factor of 2, that is, which doubles the rate of chemical reaction with 10 °C increase and corresponds to an activation energy for moisture transport in the Parylene around 50 kJ mol $^{-1}$,[12] a 6-dyad encapsulation achieves a lifetime equivalent to 5.1 \pm 0.3 years for Mg films, and 5.5 \pm 0.6 years for IDEs at 37 °C.

Stretchable optoelectronic systems (OEs) are prepared with serpentines of PI and metallic Ti/Pt/Ti tracks (Figure 2c and

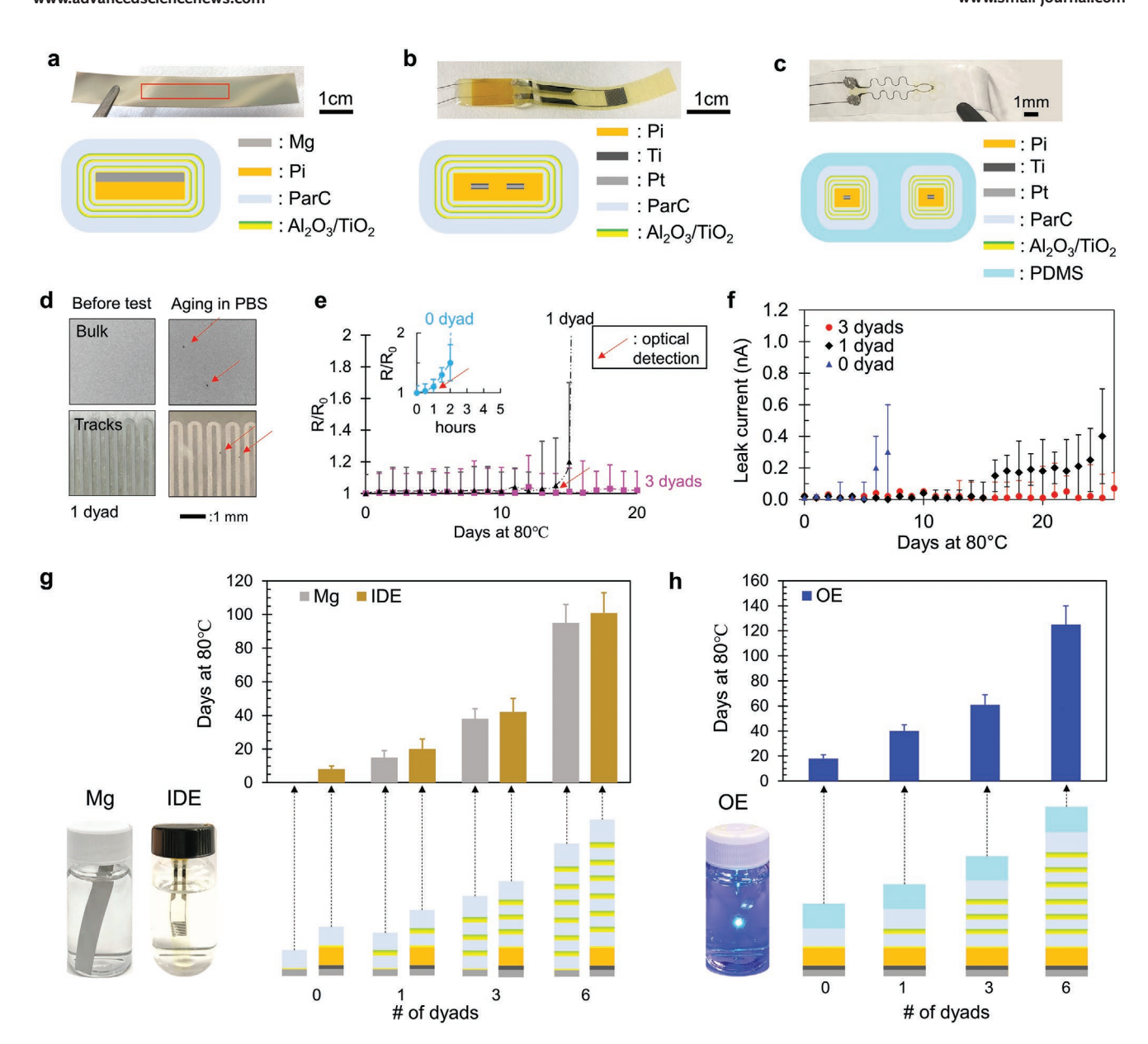


Figure 2. Lifetime evaluation of the multilayer coatings. a) A picture and a schematic of the multilayers directly coated onto Mg film, b) IDE, and c) OE device. d) Pictures of 1 dyad coated Mg bulk films and serpentine tracks before and after accelerated aging in PBS, where corrosion spots are observable, and e) relative resistance R/R_0 , where R is the resistance and R_0 is the resistance at time 0 of Mg tracks versus time. (red arrows indicate the time when the corrosion spots are first observed). f) Leakage current of representative 0, 1, and 3 dyads multilayer-coated IDEs over time. g) Lifetime of Mg films and IDEs (n = 4 per each, mean \pm s.d.) from the Mg soaking test and leakage current measurement, respectively. The schematics below describe the corresponding barrier architecture. h) Lifetimes of OEs (n = 4 per each dyad, mean \pm s.d.) from the voltage measurement. The schematics below describe the corresponding barrier constitution.

Figure S3, Supporting Information) to connect micro-LEDs; each system is then encapsulated with the multilayer coating. Upon a 5 mA bias, we monitor the micro-LED voltage over time in PBS solution at 80 °C. Similarly to the Mg and IDE samples, the performance of the OEs improves with increasing dyad number (Figure 2h). Without an ALD film coating, the OEs fail after 18 \pm 3 days in PBS (more than twice longer than the IDEs (8 \pm 2 days)). The lifetime of OEs coated with the 6-dyad encapsulation reaches 125 \pm 15 days at 80 °C, equivalent to 6.7 \pm 0.8 years at 37 °C, again, significantly longer than the IDE lifetime. These lifetime differences likely come from the much

smaller footprint of the OE interconnects compared to the IDEs (\approx 500 times in surface area, (length) \times (width)). These experimental results confirm that the coating lifetime may be extended with the introduction of ALD films and increasing the number of organic/inorganic dyads.

4. Cracking of Organic/Inorganic Multilayers

Next, we evaluate the performance of the multilayer barriers upon mechanical loading. Pristine samples prepared

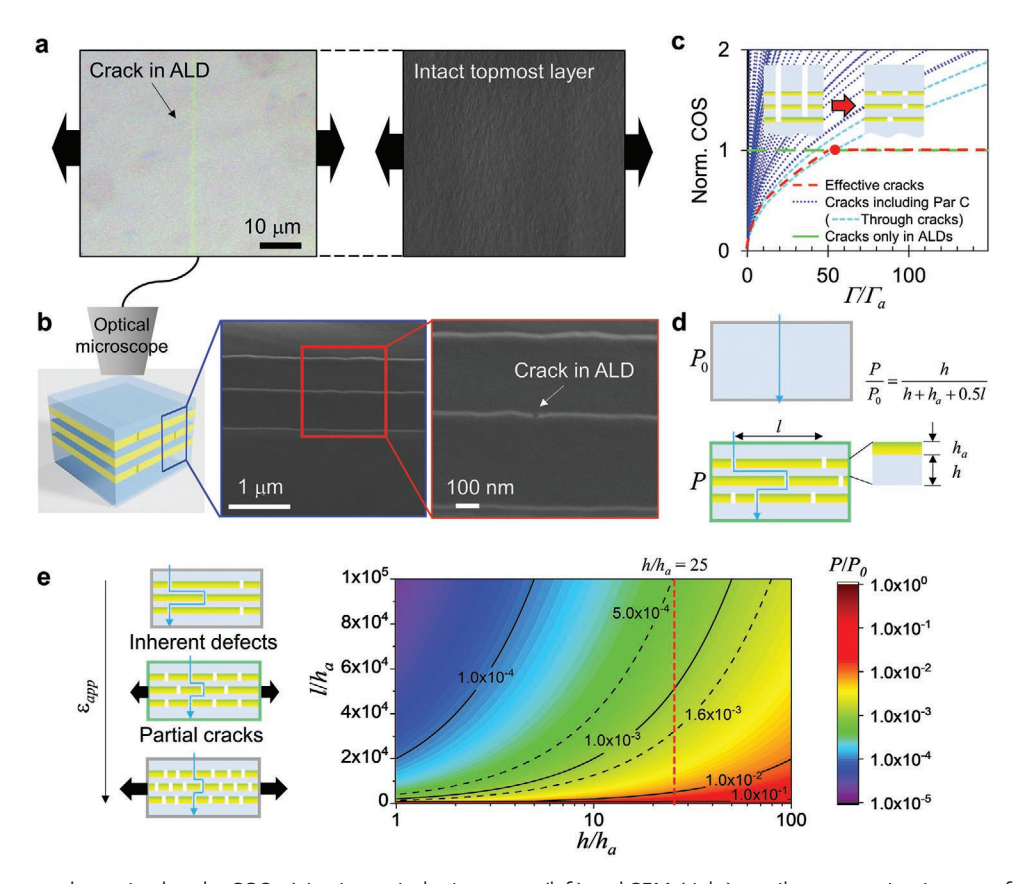


Figure 3. Multilayer stacks strained to the COS. a) In situ optical microscopy (left) and SEM (right) tensile test top view images of the same location of the multilayer film strained to COS. b) Ion-polished cross-sectional SEM images of Parylene C-Al₂O₃-TiO₂ multilayer barrier films strained to COS, presenting the whole cross-section (left) and the one focused on the tunnel crack in the middle ALD layer (right). c) A normalized COS including all possible crack configurations in 3 dyads organic/inorganic multilayers as a function of ratio of the fracture energy of Parylene C organic layer Γ to that of ALD inorganic layers Γ_a . d) An approximated relative permeability for partially cracked alternate organic/inorganic multilayer structure. Schematics of a single Parylene C layer (above) and partially cracked multilayer (below), illustrating the tortuous overall pathway preserved in the proposed design. e) Schematics of initial configuration before cracking, that is, pathway through pin-holes, and partial cracks as the strain applied. A contour plot of isopermeabilities P/P_0 mapping with the relative interlayer Parylene C thickness h/h_a in x-axis and the relative crack spacing l/h_a in y-axis. h/h_a is displayed in a log scale to highlight the transition. Red vertical dashed line indicates this work where $h/h_a = 25$.

on polyimide foil are stretched in a uni-axial stretcher until cracks become visible optically, that is, at COS, then immediately unloaded to maintain the crack configurations at COS (Figure 3a). The COS is measured to be $\varepsilon_{\rm app}=1.4\pm0.2\%$ for the multilayers independently on the number of dyads. The observation of cracks through the multilayer stack is difficult therefore cross-section imaging with SEM (Hitachi SU5000) of ion polished stacks is preferred. Figure 3b displays that organic-inorganic interfaces remain well bonded at COS, with intact Parylene C interlayers and one crack in the middle ALD layer. Throughout the entire polished cross-section, cracks are only observed in the ALD layers (Figure S4, Supporting Information).

Multiple crack configurations may occur depending on the design of dyads. We model the 3-dyad multilayer as an example and consider all failure modes within the multilayer coating, that is, 63 cases, namely tunnel cracks within the Parylene C films, through cracks from the topmost Parylene C film and brittle cracks in the ALD films. Using finite element analysis (FEA), we then compute the transition of crack configuration depending on the relative fracture energies of organic Parylene

C layers Γ to inorganic ALD layers Γ_a taken to be $\Gamma_a = 6.4 \text{ J} \cdot \text{m}^{-2}$ (Figure 3c). [20] COS is normalized to that of the ALD layers, that is, 1.4 % (Figure 3c, green line) (further details are included in the Supporting Information). Cracking through Parylene C layers preferentially occurs for Γ/Γ_a < 55. Above that threshold, cracking only occurs in the ALD layers. Therefore, the fracture energy of Parylene C is found to be over 350 J·m⁻², 55 times higher than that of ALD films. Therefore the multilayer design ensures cracks only occur in the inorganic layers and as a primary cracking mode, essentially due to the high fracture energy of the organic material compared to that of the inorganic materials. Sufficiently thick Parylene interlayers are necessary to decouple the cracking in the inorganic layers not to occur together. Our design $h/h_a = 25$, where h_a and h are the thickness of the ALD layer and Parylene C interlayer, respectively, allows the equal chance of partial cracks that can produce the tortuous diffusion pathway even after the cracking (Figure S4, Supporting Information).

This result demonstrates an extremely hindered diffusion pathway will persist in cracked multilayers due to the localized cracking in the inorganic layers (Figure 3d). The relative





permeability of the cracked Parylene C-ALD multilayer is further analyzed using Nielsen's equation, originally developed for layered clay nanocomposites. [29] Long pathways for permeating defects between the ALD layers can be perceived in the same way as a vapor detouring the clay nanoplatelets, and amount of such defects, pin-holes, and cracks can be calculated for predicting consequential barrier properties.^[23] In our case, the relative permeability P/P_0 is defined with the permeability of the cracked multilayer P and that of Parylene C P_0 as indicated in Figure 3d. As shown on the isoline map in Figure 3e, P/P_0 decreases with increasing aspect ratio of cracked ALD fragments l/h_a and decreasing relative interlayer Parylene C thickness h/h_a , where l is the crack spacing. Pristine multilayer's permeability degrades as the crack spacing decreases, however the sufficiently high crack spacings at COS and tortuous pathway through the partially cracked ALD layers likely delay the failure to a certain period of time. These decreases in the crack spacing l and in the barrier properties P accompany the same factor until the crack spacing is reduced to the comparable scale to h below a few micrometers, for example, a threefold decrease of l/h_a degrades P/P_0 by a factor of 3 (Figure 3e). Thus, the partially cracked multilayer can tolerate the direct failure even for straining over COS to a slight extent in the absence of additional failures (Figure S4, Supporting Information). Presumably, the lifetimes of both pristine and cracked multilayers increase as the number of dyads increases as long as the Parylene C and ALD/Parylene C interfaces remain intact without delamination or substrate cracking from the continuous static loading[30] or straining far over the COS (Figure S4, Supporting Information).

5. Flexible and Stretchable Substrates with Cracked Multilayers

In a follow-up set of experiments, we assess the lifetime of Mg films and OEs encapsulated with intentionally pre-cracked multilayer coating. The samples first sustain a uniaxial loading cycle to COS leading to form partial cracks in the ALD layers then are soaked in PBS solution at 80 °C for aging. A central region of 5 mm \times 3 cm at the center of the Mg samples, away from the stretcher clamps, is optically analyzed (Figure 4a). Corrosion of the strained Mg films appears as spots at the beginning due to the presence of pin-holes in the first ALD adhesion layer for all type of samples. These spots are clearly visible in the 3-dyad strained sample (Figure 4a). Multilayers with high number of dyads slow down the degradation and allow to detect such corroded spots (Figure S5, Supporting Information), while a single Parylene C encapsulation layer deteriorates rapidly, within less than a day in the absence of ALD interlayers (Figure 4a). A significantly extended lifetime from 0 through 1, 3, to 6 dyads is measured (Figure 4b). Cracked 6-dyad multilayers survive longer than non-cracked 1 dyad, that is, 35 and 15 days on average, respectively. Of note, for two out of five samples coated with cracked 6-dyad multilayers, lifetimes are comparable to that of the non-cracked 3 dyads, that is, 38 days.

We manufacture stretchable OEs so that the local maximum strain in the interconnect serpentine equals the COS when a 20 % in-plane uni-axial $\varepsilon_{\rm app}$ is applied (Figure 4c). We

assess the stretchability and lifetime of OEs coated with 0, 1, 3, and 6-dyad pre-cracked multilayers (Figure 4d). We apply the same protocol used for unstrained samples, that is, the voltage measurement over time for an applied bias current of 5 mA. Optical power changes follow the same trend as previously observed and both micro-LEDs work properly until a rapid increase of the voltage (until the compliance limit of the measurement equipment). This also provides additional information that the leakage through the multilayer previously identified in IDEs is not developed enough to reduce the optical power until the metals corrode. We obtain lifetimes equivalent to 2.1 \pm 0.4 and 3.0 \pm 0.5 years at 37 °C for the OEs encapsulated with cracked 3 and 6 dyad multilayers, respectively. A very effective tortuous diffusion path engineered from the mechanical initial stretch is thus formed and preserved within the multilayer coating throughout the measurement. Such tortuous path improves the lifetime as the number of dyads increases and prevents direct failure as predicted in Figure 3e. The lifetime of multilayers with and without containing partial cracks is compared for Mg films (Figure 4e) and OEs (Figure 4f). Both pristine and pre-cracked multilayers agree well with linear trendlines increasing at a steady rate with the increasing number of dyads. The trendline suggests the lifetime of a decade achievable with 12 dyads for Mg films and 10 dyads for OEs, respectively.

Traditional packaging designs point to "perfect", defect-free barrier coatings. Flexible, and even stretchable, (bio)electronic systems also require mechanical compliance. This practical setting ultimately requires a safe operational range governing the mechanical deformation of coated devices with consistent lifetimes. Organic/inorganic multilayers fulfill such requirements with the different approach compared to inorganic multilayers, which are typically developed for creating the perfect hermeticity in a single barrier layer. [9,10,16,31,32] We compare the COS and lifetimes of Mg films coated with inorganic multilayers and organic/inorganic multilayers, respectively, with same total thickness of the inorganic phase (Figure 5a,b, respectively). As a reminder, the COS of inorganic ultrabarrier films decreases with increasing film thickness h_f in $h_f^{-0.5}$, and thus limits the device deformability with h, whereas the barrier performance weakly improves with h as shown in Figure 5a. In contrast, decoupling inorganic layers with organic interlayers maintains the COS of the thin inorganic layers. Moreover, it enables increased lifetime with increasing number of dyads, and further allows to predict the lifetime in a predictable manner. Figure 5c further demonstrates the unique benefit of the hybrid strategy, where a substantial lifetime is maintained with the organic/inorganic multilayer barriers that have been strained to their COS (1.4% here). This is clearly not the case for the strained inorganic-only barriers that crack at once and whose lifetime is immediately lost. To further highlight the advantage of partial cracks in our design, we perform the accelerated aging test combined with cyclic stretch for OEs coated with 6 dyads after 20% strain applied (i.e., COS) to initially start with the presence of partial cracks (Figure 5d). We conduct the cyclic stretch of 500 cycles at 10% applied strain every week, and the sample is kept at 80 °C in PBS solution all the time except for less than half an hour of the cyclic stretch in PBS but at room temperature. A stable response in functionality of

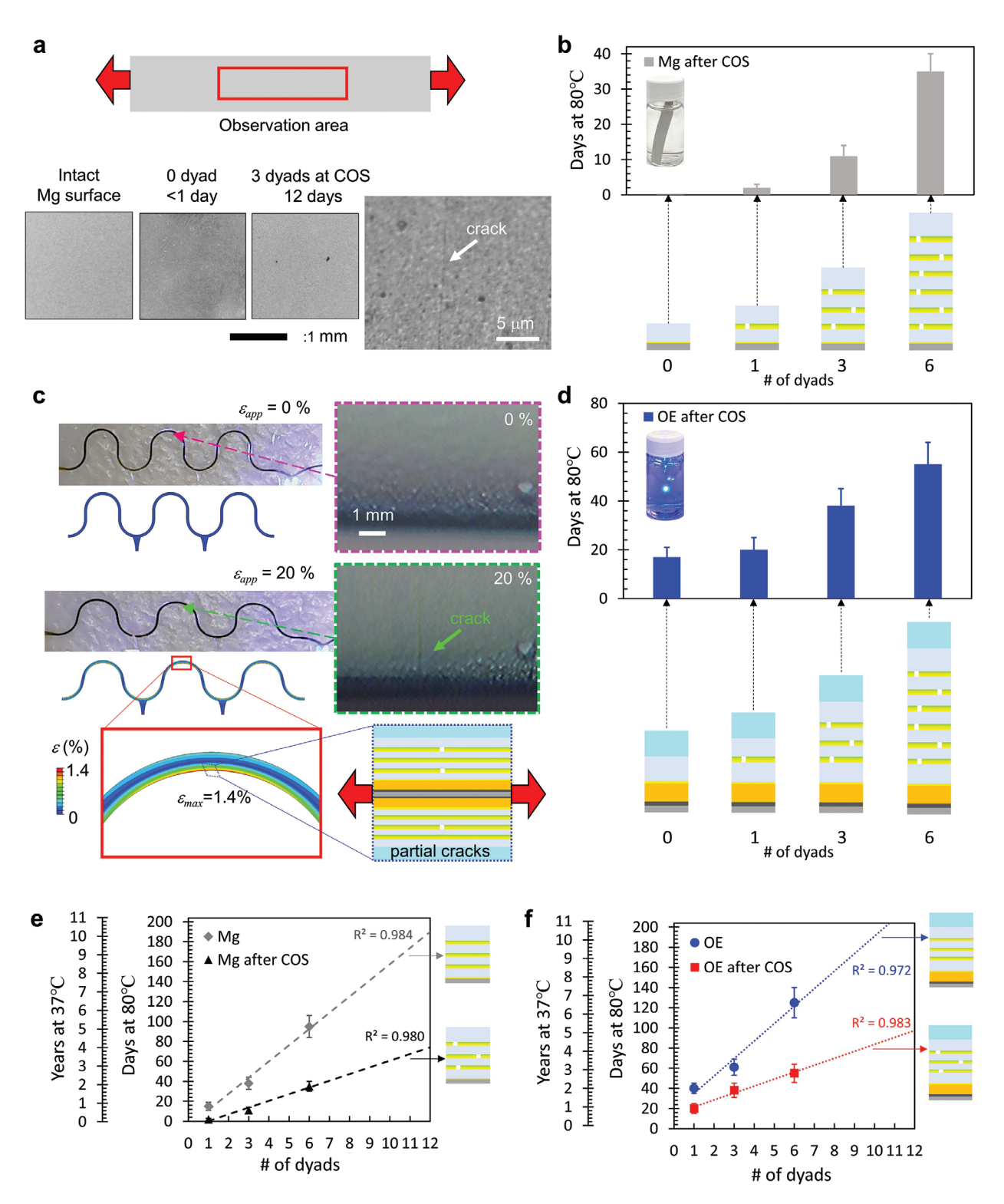


Figure 4. Hermeticity of flexible devices. a) A schematic of the Mg film with an observation area and a uniaxial loading direction indicated. Optical images of encapsulated Mg films: an intact film at day 0, 0 dyad after a day, and cracked 3 dyads after 12 days. An optical image of the channel crack in the multilayer on Mg film strained to COS. b) Lifetimes of cracked Mg films coated with multilayers. (n = 5 per each dyad, mean \pm s.d.) c) FEA and the corresponding images of fabricated stretchable OEs (half of the device is shown) and their damage morphology (optical micrographs) before and after stretch to an applied strain $\varepsilon_{\rm app}$ of 20%. A schematic of the multilayer-coated directly on the curved PI/metals/PI possessing partial cracks at COS at the location of maximum local strain is also shown. d) Lifetimes of cracked OEs encapsulated with different number of dyads. (n = 5 per each, mean \pm s.d.) e) The lifetime of Mg films at 80 °C (tested) and at 37 °C (converted) with and without containing partial cracks. f) The lifetime of OEs at 80 °C (tested) and at 37 °C (converted) with and without containing partial cracks.

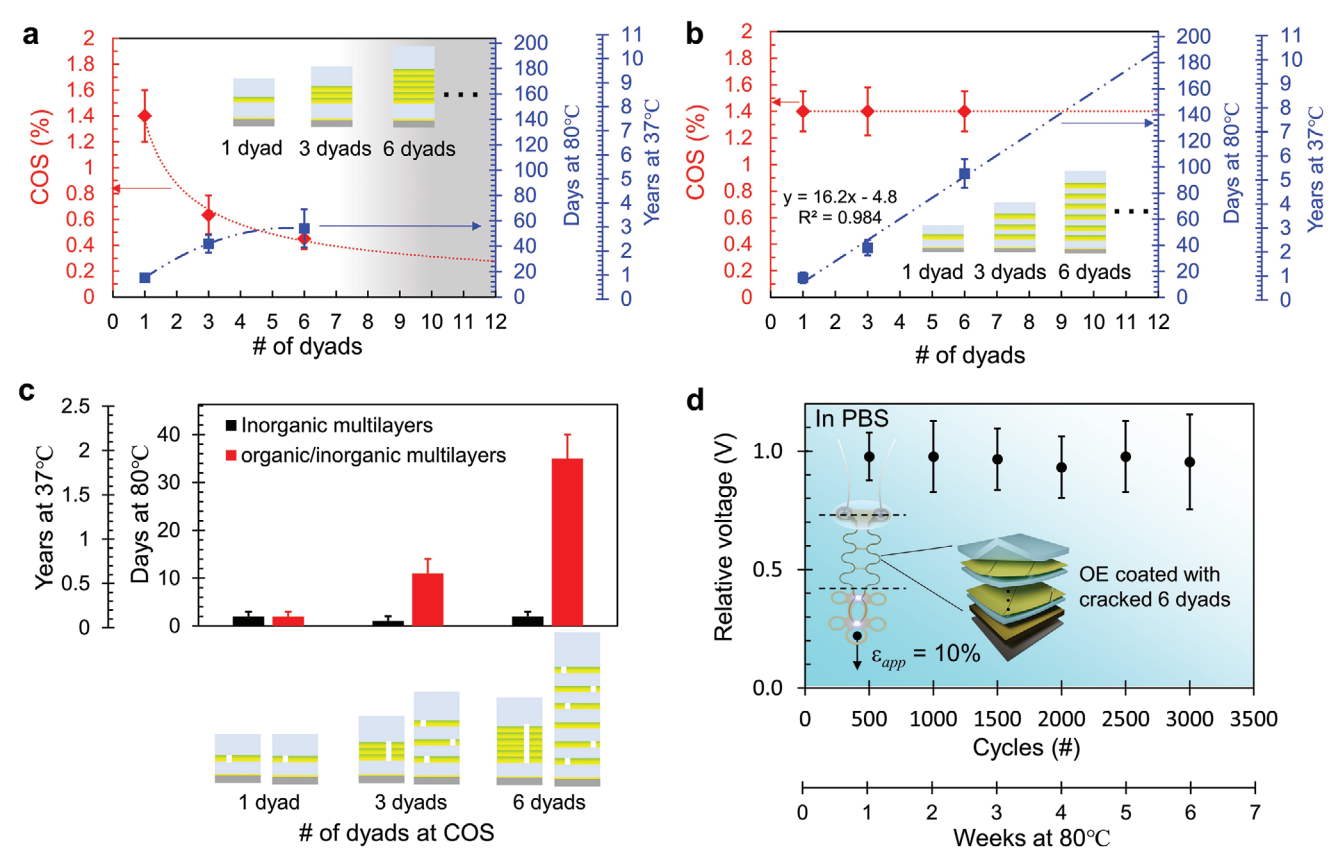


Figure 5. Organic interlayer effect on flexible and stretchable devices. Flexibility limit (COS) and lifetime of a) inorganic multilayers and b) organic/inorganic multilayers encapsulation of Mg/PI substrates. c) Lifetime comparison of encapsulated and strained Mg films for inorganic multilayers versus organic/inorganic multilayers. (n = 5 per each, mean \pm s.d.) d) Relative voltage measurement of OE coated with the cracked 6 dyads organic/inorganic multilayer under the accelerated aging in PBS with cyclic stretch at 10% strain over time, that is, 500 cycles accumulated each week.

the micro-LEDs signifies the extended lifetime to failure under combined dynamic loadings. This result also demonstrates that the operation under the applied strain below COS does not critically extent damages.

6. Conclusion

In conclusion, hybrid organic-inorganic coatings are a promising technological route for the safe and robust packaging of mechanically compliant and microfabricated devices. Parylene C with high enough fracture energy and thickness allows to constrain cracking only in ALD Al₂O₃/TiO₂ inorganic layers at the COS. The partially cracked organic/inorganic multilayer behaves similarly to perfectly aligned nanoplatelet polymer composites^[33] as the extended lifetimes are found in Mg corrosion test and OE devices lifetime measurement. The organic/inorganic multilayer technology platform reported herein enables further extension of the stacks to include 10 and 20 dyads, in order to achieve longer lifetimes, without compromising COS and ensuring a safe barrier performance even after cracking. In particular, the deposition process does not require a high temperature and thus encapsulates the product without temperature constraints. Eventually, integrating the organic/inorganic multilayer system that leads to

partial cracks with the inorganic layer towards pin-hole free will synergize the advantages in both approaches: creating perfect layer and maintaining tortuous pathways. Further optimization of the tortuosity in the diffusion model^[34] and the degree of lifetime decrease depending on the frequency of continuous electrical powering are promising follow-up studies, and more importantly, stretchability of OEs can be increased as well without doubt through the design optimization, for example, out-of-plane deflection^[27] and pre-strained encapsulation.^[35] However, this is beyond the scope of the current work. The process versatility enables therefore tailoring barrier layer designs according to the application needs in terms of expected lifetime.

7. Experimental Section

Deposition of Multilayer Barrier: All depositions were completed in a single chamber, from Comelec C30H equipment platform. CVD Parylene C was deposited at a temperature of 30 °C. For the ALD layers, temperature was limited to 100 °C to minimize thermal annealing effects of the Parylene C films; each gas precursor was utilized with nitrogen (N2) as the purge gas. The growth per cycle for Al2O3 and TiO2 were 1.7 and 0.76 Å, respectively. To prepare free-standing barrier coatings, the glass surface was initially cleaned and coated with a demolding agent (Micro-90, Sigma-Aldrich) to lift-off the complete Parylene C-dyads-Parylene C multilayer structure (Figure 1d). Mg films, wired, fabricated



IDE, and OE samples were hung in the chamber to coat conformally under the stabilized pressure. A tiny hole was pierced on one end of the Mg film to hang in the chamber.

WVTR Measurement: WVTRs of the single- and multi-layer structures on 25 μm Parylene C as a base substrate were measured at 38 °C and 50% RH (relative humidity) using a permeation cell (Systech Instrument 7001) with a detection limit of $2\times 10^{-2}~g\cdot m^{-2}\cdot day^{-1}.$ WVTR of 25 μm Parylene C was calculated to be 0.5 $g\cdot m^{-2}\cdot day^{-1}.$ Films grown on the glass substrate were detached (Figure 1d) and strained to produce mechanical damages as shown in Figure 1a, followed by the WVTR measurement.

Mg Evaporation: 250 nm Mg was evaporated on to the prepared on 50 μ m thick polyimide foil, followed by a laser-cut of the substrate to a size of 1 cm \times 6 cm rectangle.

Leakage Current Measurement and Electrochemical Impedance Spectroscopy: DC current was measured using a sourcemeter (Keithley 2400) while applying a pulse of 5 V for 10 s, and the insulation was designated as failed if the currents exceeded 1 nA. For the EIS measurement, each IDE finger was connected with counter/reference and working/working sense terminals (two-electrode setup) and the values were measured from a potentiostat (Gamry instruments). [36]

Opto-Electrical Properties Measurement: The total optical power at 470 nm was measured with a large photodiode (S170C, Thorlabs) and a power meter console (PM100D, Thorlabs). Given a minimum forward voltage 2.8 V at 20 mA from the LED supplier datasheet, we estimate the array series wiring resistance \approx 210 Ω .

Micro-LED Integration on a Flexible Substrate: Micro-LEDs ($240 \times 320 \times 140~\mu m^3$, DA2432, Cree Inc.) were aligned on a glass slide with their connection pads facing down. Sn/Bi/Ag solder paste (SMDLTLFP10T5, Chipquik) bumps were dispended to the connection pads exposed on patterned Si wafer, followed by the deposition of LEDs onto the solder paste using a pick-and-place equipment (JFP Microtechnic). The solder paste reflow at 138 °C ensured mechanical and electrical connections. A 14 % weight ratio solution of polyisobutylene (PIB, Oppanol, BASF) in cyclohexane (Sigma-Aldrich) was drop-casted on the micro-LED surface. The solvent evaporation (3 min at 60 °C) was followed by the overnight curing at room temperature. After the multilayer barrier encapsulation, the micro-LEDs were encapsulated with a bulk PDMS (>200 μ m, Sylgard 184, Dow Corning). This allowed the deformation constrained to the in-plane and thus enabled to catch COS immediately during the in situ microscopy tensile test.

In Situ Microscopy Tensile Test: The Mg films and OEs were strained in a portable tensile stage (Linkam TST350) at a rate of 0.025%·s⁻¹ until observing the first crack propagations (i.e., COS) in an optical microscope (Olympus BX60).^[37] 5 nm Au was sputtered for the top layer observation in SEM, and manual uniaxial stretcher was applied for in situ SEM tensile test separately.

Ion-Polish of Multilayer Cross-Section: A tested sample strained to COS was embedded in the epoxy embedding medium (45359-1EA-F, Sigma-Aldrich). The cross-sectional surface was polished with polisher (ILION II x-section, Gatan, Inc.) at gun angle of 1° , single sectorial rotation angle of 90° , low temperature -100 °C, and at 5 kV for 2 h first and then 3 kV for 3 h. 10 nm carbon was coated for cross-section observation to reduce charging effects.

FEA for Stretchable OE Circuits: Identical dimensions of the 2D laminated structure and elastic-plastic material properties were implemented for metals, PI, Parylene C, and ALD multilayers, followed by 3D encapsulation with 200 μ m PDMS assuming Neo-Hookean hyperelastic behavior. 4-node shell elements with the multilayer (3 dyads-Parylene C/ALD/PI/metal/PI/3 dyads-Parylene C/ALD) composite modeled the 3D conductors, and 8-node solid elements modeled the final sealing with elastomer. Refined mesh with mesh convergence verified the computational accuracy using commercial software (ABAQUS). The evaluation result of experimented stress-train data for hyperelastic properties of the PDMS encapsulation gave the relevant material parameter ($C_{10} = 0.805$ MPa). The other material parameters used were: E = 4.0 GPa, $\nu = 0.27$ for both polyimide and Parylene C; and $E_{metal} = 150$ GPa, $\nu_{metal} = 0.27$ for Ti/Pt/Ti metal tracks; $E_a = 150$ GPa, $\nu_a = 0.23$ for ALDs.

Supporting Information

Supporting Information is available from the Wiley Online Library or from the author.

Acknowledgements

The authors would like to acknowledge financial support by the Bertarelli Foundation, the SNSF grant 200021_182055, and InnoSuisse grants 25575.1 PFIW-IW and 45944.1 IP-ENG. The authors would like to thank the staff at the Neural Microsystems Platform of the Wyss Center for Bio and Neuroengineering for their help with the fabrication processes, and the staff of EPFL CIME for assistance in samples' preparation.

Conflict of Interest

The authors declare no conflict of interest.

Author Contributions

S.P.L. and Y.L. conceptualized the work and supervised the project. F.B. and M.V. developed the deposition process line. S.P.L., Y.L., and F.B. acquired funding and managed project. K.K. and K.W. fabricated samples and M.V. encapsulated samples with proposed designs. G.S., K.K., and K.W. conducted verification and data curation for the lifetime assessment of the samples. K.K. and J.C. conducted investigations, verification, and data curation for the mechanical characterization of the samples. K.K. developed a methodology, conducted data analysis, performed simulations. K.K., S.P.L, and Y.L. wrote the original draft. All authors contributed to reviewing and editing the manuscript.

Data Availability Statement

Research data are not shared.

Keywords

atomic layer deposition, crack onset strains, flexible interdigitated electrodes, organic/inorganic multilayers, stretchable conductors

Received: May 25, 2021 Revised: August 3, 2021 Published online: September 3, 2021

^[1] S. P. Lacour, G. Courtine, J. Guck, Nat. Rev. Mater. 2016, 1, 16063.

^[2] L.-H. Shi, F. Luo, D. J. Woodward, J.-Y. Chang, Synapse 2006, 59,

^[3] K. C. Cheung, P. Renaud, H. Tanila, K. Djupsund, Biosens. Bioelectron. 2007. 22. 1783.

^[4] R. P. von Metzen, T. Stieglitz, Biomed. Microdevices 2013, 15, 727.

^[5] E. M. Schmidt, M. J. Bak, J. S. McIntosh, Exp. Neurol. 1976, 52, 496.

^[6] C. Metallo, R. D. White, B. A. Trimmer, J. Neurosci. Methods 2011, 195, 176.

^[7] I. R. Minev, P. Musienko, A. Hirsch, Q. Barraud, N. Wenger, E. M. Moraud, J. Gandar, M. Capogrosso, T. Milekovic, L. Asboth, R. F. Torres, N. Vachicouras, Q. Liu, N. Pavlova, S. Duis, A. Larmagnac, J. Voros, S. Micera, Z. Suo, G. Courtine, S. P. Lacour, Science 2015, 347, 159.





- [8] H. Fang, J. Zhao, K. J. Yu, E. Song, A. B. Farimani, C.-H. Chiang, X. Jin, Y. Xue, D. Xu, W. Du, K. J. Seo, Y. Zhong, Z. Yang, S. M. Won, G. Fang, S. W. Choi, S. Chaudhuri, Y. Huang, M. A. Alam, J. Viventi, N. R. Aluru, J. A. Rogers, *Proc. Natl. Acad. Sci. U. S. A.* 2016, 113, 11682.
- [9] E. Song, H. Fang, X. Jin, J. Zhao, C. Jiang, K. J. Yu, Y. Zhong, D. Xu, J. Li, G. Fang, H. Du, J. Zhang, J. M. Park, Y. Huang, M. A. Alam, Y. Mei, J. A. Rogers, Adv. Electron. Mater. 2017, 3, 1700077.
- [10] E. Song, R. Li, X. Jin, H. Du, Y. Huang, J. Zhang, Y. Xia, H. Fang, Y. K. Lee, K. J. Yu, J.-K. Chang, Y. Mei, M. A. Alam, Y. Huang, J. A. Rogers, ACS Nano 2018, 12, 10317.
- [11] H.-P. Phan, Y. Zhong, T.-K. Nguyen, Y. Park, T. Dinh, E. Song, R. K. Vadivelu, M. K. Masud, J. Li, M. J. A. Shiddiky, D. Dao, Y. Yamauchi, J. A. Rogers, N.-T. Nguyen, ACS Nano 2019, 13, 11572.
- [12] S. Minnikanti, G. Diao, J. J. Pancrazio, X. Xie, L. Rieth, F. Solzbacher, N. Peixoto, *Acta Biomater.* 2014, 10, 960.
- [13] F. Fallegger, G. Schiavone, S. P. Lacour, Adv. Mater. 2020, 32, 1903904.
- [14] G. Schiavone, S. P. Lacour, Sci. Transl. Med. 2019, 11, eaaw5858.
- [15] M. Y. Rotenberg, B. Tian, Nat. Biomed. Eng. 2017, 1, 0048.
- [16] J. Jeong, F. Laiwalla, J. Lee, R. Ritasalo, M. Pudas, L. Larson, V. Leung, A. Nurmikko, Adv. Funct. Mater. 2019, 29, 1806440.
- [17] E. Song, Y. K. Lee, R. Li, J. Li, X. Jin, K. J. Yu, Z. Xie, H. Fang, Y. Zhong, H. Du, J. Zhang, G. Fang, Y. Kim, Y. Yoon, M. A. Alam, Y. Mei, Y. Huang, J. A. Rogers, Adv. Funct. Mater. 2018, 28, 1702284.
- [18] J. Lewis, Mater. Today 2006, 9, 38.
- [19] S.-H. Jen, J. A. Bertrand, S. M. George, J. Appl. Phys. 2011, 109, 084305.
- [20] K. Kim, O. N. Pierron, S. Graham, J. Appl. Phys. 2019, 125, 045301.
- [21] Y. Leterrier, Prog. Mater. Sci. 2003, 48, 1.
- [22] K. Kim, H. Luo, A. K. Singh, T. Zhu, S. Graham, O. N. Pierron, ACS Appl. Mater. Interfaces 2016, 8, 27169.
- [23] G. L. Graff, R. E. Williford, P. E. Burrows, J. Appl. Phys. 2004, 96, 1840.

- [24] J. Wu, F. Fei, C. Wei, X. Chen, S. Nie, D. Zhang, W. Su, Z. Cui, RSC Adv. 2018, 8, 5721.
- [25] K. Kim, X. Jia, C. Fuentes-Hernandez, B. Kippelen, S. Graham, O. N. Pierron, ACS Appl. Nano Mater. 2019, 2, 2525.
- [26] A. I. Abdulagatov, Y. Yan, J. R. Cooper, Y. Zhang, Z. M. Gibbs, A. S. Cavanagh, R. G. Yang, Y. C. Lee, S. M. George, ACS Appl. Mater. Interfaces 2011, 3, 4593.
- [27] F. Michoud, C. Seehus, P. Schönle, N. Brun, D. Taub, Z. Zhang, A. Jain, I. Furfaro, O. Akouissi, R. Moon, P. Meier, K. Galan, B. Doyle, M. Tetreault, S. Talbot, L. E. Browne, Q. Huang, C. J. Woolf, S. P. Lacour, *Nat. Biotechnol.* 2021, 39, 179.
- [28] X. Xie, L. Rieth, R. Caldwell, S. Negi, R. Bhandari, R. Sharma, P. Tathireddy, F. Solzbacher, Biomed. Microdevices 2015, 17, 1.
- [29] L. E. Nielsen, J. Macromol. Sci., Chem. 1967, 1, 929.
- [30] K. Kim, H. Luo, T. Zhu, O. N. Pierron, S. Graham, Sci. Rep. 2018, 8, 4560
- [31] E. Marin, L. Guzman, A. Lanzutti, W. Ensinger, L. Fedrizzi, Thin Solid Films 2012, 522, 283.
- [32] A. A. Dameron, S. D. Davidson, B. B. Burton, P. F. Carcia, R. S. McLean, S. M. George, J. Phys. Chem. C 2008, 112, 4573.
- [33] M. A. Priolo, D. Gamboa, K. M. Holder, J. C. Grunlan, Nano Lett. 2010, 10, 4970.
- [34] M. Schaepkens, T. W. Kim, A. Gün Erlat, M. Yan, K. W. Flanagan, C. M. Heller, P. A. McConnelee, J. Vac. Sci. Technol., A 2004, 22, 1716.
- [35] K. Li, X. Cheng, F. Zhu, L. Li, Z. Xie, H. Luan, Z. Wang, Z. Ji, H. Wang, F. Liu, Y. Xue, C. Jiang, X. Feng, L. Li, J. A. Rogers, Y. Huang, Y. Zhang, Adv. Funct. Mater. 2019, 29, 1806630.
- [36] G. Schiavone, X. Kang, F. Fallegger, J. Gandar, G. Courtine, S. P. Lacour, Neuron 2020, 108, 238.
- [37] K. Kim, S. Graham, O. N. Pierron, Rev. Sci. Instrum. 2017, 88, 036102.